The low infrared emissivity of $Ce_{1-x}Y_xO_{2-x/2}$ samples at high-temperature contributed by enhanced conductivity

Honghan Bu, Chuyang Liu*, Guoyue Xu, Yong Jiang, Tengchao Guo and Jianchao Zhang

College of Material Science and Technology, Nanjing University of Aeronautics and Astronautics, Jiang Jun Street 29, Nanjing 211106, China

Abstract: The $Ce_{1-x}Y_xO_{2-x/2}$ samples were synthesized with different doping amount by solid state reaction method. Phase structures of the samples were analyzed and characterized by XRD. The effects of different doping amount on infrared emissivity properties at 3-5μm wavebands were investigated systematically. It is found that the powder with doping molality of x=0.2 exhibits the lowest infrared emissivity value ca. 0.21 when the test temperature is 600 ℃. The mechanism for the low infrared emissivity is explored thoroughly. The reduction of infrared emissivity with increasing temperature is ascribed to the enhancement of electrical conductivity. Our results suggest that $Ce_{1-x}Y_xO_{2-x/2}$ powder with x=0.2 is a potential candidate for stealth material of aircraft engines.

1. Introduction

The infrared (IR) radiation of an aircraft is one of the most important factors which affect the detection range of an IR detection system **[1]**. In general, IR radiation from a specific exhaust system can be attributed to two parts: hot plume IR radiation and high temperature engine parts IR radiation, such as that of nozzle, and turbine blades **[2]**. As for Aircraft engine, it usually produces strong infrared radiation because of its high working temperature, which renders the aircraft easily exposed to the enemy **[3]**. Therefore, in order to improve the survivability of military targets on the battlefield, it is important to develop the materials with low emissivity at high temperature.

As well known, CeO_2 with fluorite structure exhibits high refractive index and dielectric constant **[4]** and, therefore, it is a promising material with low infrared emissivity **[5]**. As reported, the value of infrared emissivity reaches 0.3 at 600℃ after heat treatment **[6]**. However, as a stealth material, its infrared emissivity of 0.3 is still slightly higher, which is far from sufficient for engineering applications. The main factor influencing infrared emissivity is the conductivity of materials **[7, 8]**, so improving the conductivity of the material is beneficial to reducing the infrared emissivity of the material.

Doping can improve the conductivity of metal oxides **[9, 10]**. Therefore, in order to improve the conductivity of CeO_2 samples, doping is the most effective and convenient method. The ionic radius of Ce^{4+} is 92 pm **[11]**. In order to reduce the effect of lattice distortion on the conductivity of CeO_2 samples, Y^{3+} ions (90 pm) with similar radii to Ce^{4+} ions are the appropriate doping ions **[12]**. Herein, we proposed the Y^{3+} ions doped CeO_2 samples via solid state reaction method in this work, and the influences of doping molality on conductivity and infrared emissivity are discussed in detail.

*Corresponding author: liuchuyang@nuaa.edu.cn

2. Experimental details

2.1 The preparation of $Ce_{1-x}Y_xO_{2-x/2}$ samples

The doped oxides $Ce_{1-x}Y_xO_{2-x/2}$ were prepared by solid state reaction method. CeO_2 samples and Y_2O_3 samples were mixed before calcination. This mixture was gently ground in an agate mortar for homogenization. The obtained samples were calcined for 4 h in furnace at 1500 ℃ with a step of 100 ℃ with a constant heating rate of 4 ℃/min until reach the annealing temperature. After annealed, the samples were cooled to room temperature gradually in furnace. Finally, the pre-treated $Ce_{1-x}Y_xO_{2-x/2}$ samples with different x values were obtained. The values of x in $Ce_{1-x}Y_xO_{2-x/2}$ were 0.05, 0.10, 0.20 and 0.30.

2.2 The resistance test of $Ce_{1-x}Y_xO_{2-x/2}$ samples

2.2.1 The preparation of test samples

8% polyvinyl alcohol solution was added into the prepared $Ce_{1-x}Y_xO_{2-x/2}$ samples. Then the samples was pressed into Φ = 10 mm cylindrical semi-finished product, as seen in Fig. 1. To reduce the impact of contact resistance on test results, a layer of conductive silver pulp was coated on the surface of test samples. The test samples were put into the muffle furnace at 800 ℃ for 30 min, making silver layer firmly adhere to the sample surface.

2.2.2The resistance test of samples

The resistance values of doping samples were examined by YX-381TR pointer type digital multimeter. In order to ensure good contact between wire and sample at high temperature, a set of resistance testing molds were designed by me. The structure diagram is shown in Fig.1

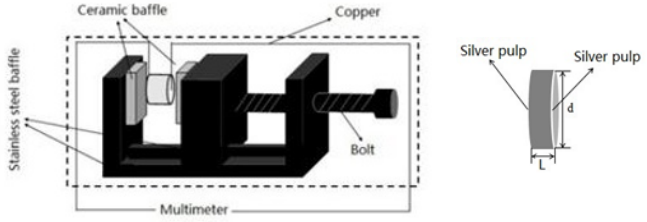

Fig.1 Resistance test mold and the sample of test

*2.2.3 The calculation of conductivity **[13]***

$$\sigma = \frac{1}{R} * \frac{L}{S} = \frac{4L}{\pi R d^2} \qquad (1)$$

Where R is the obtained resistance, L is the sample thickness, S represents electrode area. According to a typical Arrhenius type behavior which is a thermally activated process, the electrical conductivity is used to perform a plot of the Arrhenius equation.

$$\sigma = \sigma_0 exp\left(-\frac{E_a}{kT}\right) \qquad (2)$$

Where σ_0 is the pre-exponential factor, Ea is activation energy, k is the Boltzmann constant.

2.3 The infrared emissivity testing of samples

The infrared emissivity in the range of 3-5μm in different temperature was detected by an infrared emissometer (IR-2 double-band emissometer, Shanghai Institute of Technical Physics, CAS, China). The testing temperature ranges from 25 ℃ to 600 ℃ with a heating rate of 20 K•min^{-1}.

3. Results and discussion

3.1. X-ray diffraction study (XRD)

Fig. 2a shows the XRD diffraction spectra of samples with different doping amounts. Clearly, the diffraction of peaks corresponded to (111), (200), (220) and (311) planes are observed in all samples, in good agreement with the face-centered cubic fluorite structure of CeO_2 with space group Fm–3m (JCPDS card No. 34-0394) **[14, 15]**. After the introduction of Y^{3+} to CeO_2, no characteristic diffraction peaks assigned to Y_2O_3 phase is observed, indicating that Y^{3+} could enter into the CeO_2 lattice to form $Ce_{1-x}Y_xO_{2-x/2}$ solid solution oxides **[16]**.

Fig. 2b is an enlarged figure of the XRD diffraction spectra. It can be seen that the main diffraction peak at (111) have a little shift to higher angles, and with the increasing doping amount, the shift gradually increases.

The lattice constant (a) of crystalline powder can be obtained by removing the systematic errors of both un-doped and doped CeO_2 through the construction of Nelson-Riley (NR) plots **[17]**. The lattice constant of both un-doped and Y-doped CeO_2 samples measured in the present experiments is in good agreement with the theoretical values reported by Vanpoucke et al. **[18]**, shown in Table 1. The substitution of Ce^{4+} ions with Y^{3+} ions diminishes the lattice constant from 5.48 Å to 5.36 Å, and this is due to Y^{3+} ion have smaller

ionic radius than that of Ce^{4+} ion **[19]**.

For Fluorite structure of CeO_2, it has the relation for the cubic system **[20]**

$$\frac{n\lambda}{2sin\theta} = \frac{a}{\sqrt{h^2+k^2+l^2}} \qquad (3)$$

Where, n = positive integer, λ = wavelength of the incident wave, (h k l) = Miller indices, a = lattice constant. The lattice constant (a) is inversely proportional to diffraction angle θ. As a result, the decreasing lattice constant a results in an increasing diffraction angles θ.

In a word, the result strongly confirms that the Y^{3+} does replace the Ce^{4+} in the CeO_2 lattice.

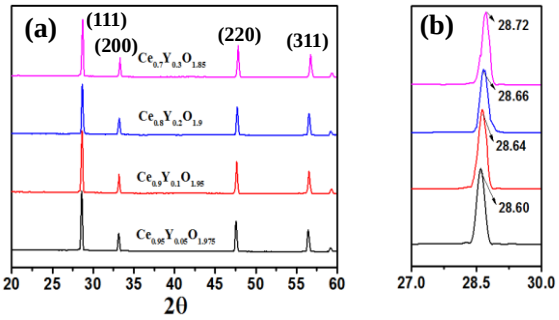

Fig.2 The XRD diffraction spectra of $Ce_{1-x}Y_xO_{2-x/2}$ samples (a) 20-60° of 2θ (b) 27-30° of 2θ

Table 1 Lattice constant of samples with different doping amounts

X values	Lattice Constant a (Å)
0	5.48
0.05	5.46
0.1	5.43
0.2	5.41
0.3	5.36

3.2 The infrared emissivity and conductivity of $Ce_{1-x}Y_xO_{2-x/2}$.

Fig. 3 summarizes the infrared emissivity values of the samples in 3-5μm waveband in the different temperature ranges. It can be clearly found that the infrared emissivity of all samples decreases significantly with the temperature rising from 30 ℃ to 600 ℃. Further, the infrared emissivity values reduce gradually from x=0 to x=0.2, while increases gradually from x=0.2 to x=0.3.

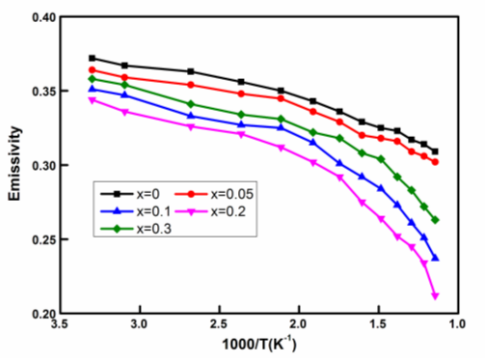

Fig. 3The infrared emissivity values of $Ce_{1-x}Y_xO_{2-x/2}$ samples

Simultaneously, the electrical conductivity (Fig. 4) of all samples was tested at above temperature range. The results show that change tendency of electrical conductivity values is contrary to the change tendency of infrared emissivity. With the increasing temperature, electrical conductivity of all samples increases significantly. Additionally, the electrical conductivity values increase gradually from x=0 to x=0.2, while decrease from x=0.2 to x=0.3.

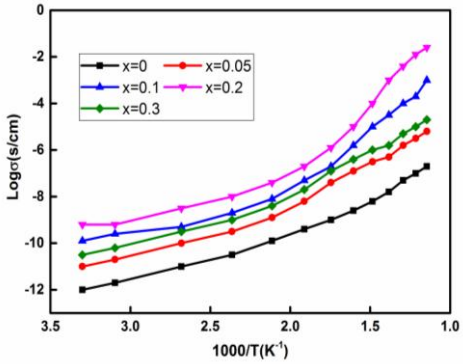

Fig. 4 The electrical conductivity of $Ce_{1-x}Y_xO_{2-x/2}$ samples

3.3 The influences of doping amount on the conductivity of $Ce_{1-x}Y_xO_{2-x/2}$ samples

When the Y^{3+} replaced the Ce^{4+} in the CeO_2 lattice, oxygen vacancy (V_o) defects occurred at once. The defect reaction follows the principle of charge conservation. The effective negative charge of Y'Ce can be compensated in three different ways, which are closely related to the intrinsic defect reaction:

$$M_2O_3 \xrightarrow{2CeO_2} 2M'_{Ce} + 3O_o + V_o^{\bullet\bullet}$$

$$2M_2O_3 \xrightarrow{CeO_2} 3M'_{Ce} + M_i^{\cdots} + 6O^{\times}_o$$

$$Ce^{\times}_{Ce} + O^{\times}_o + 2M_2O_3 \xrightarrow{CeO_2} 4M'_{Ce} + Ce_i^{\cdots\cdots} + 8O^{\times}_o$$

As reported, the V_o compensation form is the optimal compensation form as for rare earth element cation with large radius **[21]**. With the increasing doping amount, more Y^{3+} replaced the $Ce^{4+,}$ therefore, more V_o were produced, which greatly increases the ionic conductivity of the materials **[22]**. However, when the doping molarity reaches a certain level, the conductivity begins to deteriorate, which is ascribed to the changes in transition types of V_o, as shown in Fig. 5 **[23]**. The corresponding transition energy was calculated according to the literature **[24]** and the results are summarized in Table 2. It is pointed that lower transition energy of V_o can lead to easier transition of V_o.

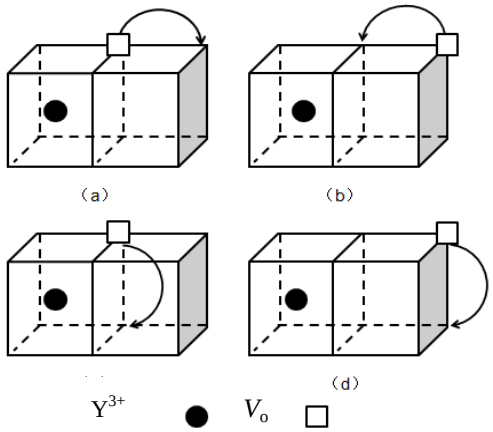

Fig. 5 Transition type of oxygen vacancy

Table 2 The transition types and transition energy of oxygen vacancy

	transition types of V_o	transition energy of V_o
(a)	$1^{st} \longrightarrow 2^{nd}$	0.31
(b)	$2^{nd} \longrightarrow 1^{st}$	0.22
(c)	$1^{st} \longrightarrow 1^{st}$	0.57
(d)	$2^{nd} \longrightarrow 2^{nd}$	0.20

When CeO_2 has lower Y^{3+} doping amount, V_o is mainly located in the 2^{nd} and it results in more easier transition of V_o. In this case, more V_o were produced with the increasing doping amounts, which contributes to the improvement of conductivity of doped samples. When Y_2O_3 doping amount reaches a certain value, the Vo located in 2^{nd} up to the maximum value, which results in the maximum conductivity. Afterwards, Y_2O_3 doping amount continue to increase, more Y^{3+} occupied Ce^{4+} ion in lattice position, causing the original V_o located in 2^{nd} gradually converting into the V_o located in 1^{st} of new Y^{3+}. Obviously, it is difficult for V_o to transition because of higher transition energy, which leads to the decreasing of conductivity.

3.4 Mechanism for enhanced conductivity of $Ce_{1-x}Y_xO_{2-x/2}$ samples under elevated temperature

As shown in Fig. 4, the curves of lgσ -1000/T of all doped samples show an increasing linear relationship, which indicates that the conductivity of doped samples improves gradually with the increasing temperature. As reported, the electrical conductivity can be expressed as the following equation **[25]**

$$\sigma = nq\mu \qquad (4)$$

Where n is the concentration of the intrinsic charge carriers, μ is the mobility of charge carriers. With the temperature rising, μ has no obvious change, while the intrinsic excitation of CeO_2 increases rapidly and the concentration of the thermally activated intrinsic charge carriers increases rapidly, which results in the sharp increasing of electrical conductivity **[26]**.

4. Conclusions

The $Ce_{1-x}Y_xO_{2-x/2}$ samples are prepared successfully by solid state reaction method. The X-ray diffraction study confirms that the synthesized $Ce_{1-x}Y_xO_{2-x/2}$ samples have cube fluorite structure. The suitable doping of Y^{3+} ions is conducive to improving the conductivity of metal oxide CeO_2, which leads to the reduction of the infrared emissivity in CeO_2. When the doping amount of Y^{3+} increases from 0.05 to 0.2, the electrical conductivity of $Ce_{1-x}Y_xO_{2-x/2}$ samples rises gradually. But the conductivity of $Ce_{1-x}Y_xO_{2-x/2}$ samples diminished afterwards with the doping amount increasing from 0.2 to 0.3. The conductivity value is the lowest at the doping amount of x=0.2, which results in the lowest infrared emissivity reaching 0.21. Obviously, the $Ce_{1-x}Y_xO_{2-x/2}$ powder with x=0.2 has great potential applications for adaptive camouflage in infrared waveband.

Acknowledgements

This research is financially supported by the National Natural Science Foundation of China (Grant Nos: 51173079) and a project funded by the Priority Academic Program Development of Jiangsu Higher Education Institutions (PAPD).

References

[1] E. Coiro, J. Aircr., **50**, 103 (2013)

[2] T. Zhou, Q. Wang, T. Li, Chin. J. Aeronaut., **30**, 651 (2017)

[3] O. Michailovich, D. Adam, IEEE T. Med. Imaging, **22**, 368 (2003)

[4] J. P. Huang, Y. B. Li, X. D. He and et al, Appl. Surf. Sci., **259**, 301(2012)

[5] R. Siegle, J. R. Howell. Thermalradiation heat transfer. McGraw-Hill Book Company. 1 (1972)

[6] Y. Jiang, G. Y. Xu, T. C. Guo and et al, Infrared Technol., **33**, 699 (2011) in Chinese.

[7]T. G. Guo, G. Y. Xu, S. J. Tan and et al, Mater. Res. Bull. **95**, 354 (2017).

[8] X. X. Yan, Y. T. Cai, R. Lu and et al, Int. J. Polym. Sci., **2017**, 5017356 (2017).

[9] U. Godavarti, V. D. Mote, M. Dasari, J. Asian Ceram. Soc., **5**, 391 (2017)

[10] M. Gupta, S. Shirbhate, P. Ojha and et al, Solid State Ionics, **320**, 199 (2018)

[11] H. Muta, Hi. Kado, Y. Ohishi and et al, J. Nucl. Mater., **483**, 192 (2017)

[12]P. Gupta, R. Nagarajan, Materialstoday Chem., **7**, 15 (2018)

[13]W. Lerdprom, C. Li, D. D. Jayaseelan and et al, J. Eur. Ceram. Soc., **37**, 343 (2017)

[14] Y. N. Liao, L. F. He, C. G. Man and et al, Chem. Eng. J., **256**, 439 (2014)

[15]T. Désaunay, G. Bonura, V. Chiodo and et al, J. Catal., **297**, 193 (2013)

[16] X. Y. Feng, J. X. Guo, X. R. Wen and et al, Appl. Surf. Sci., **445**, 145 (2018)

[**17]** J. B. Nelson, D. P. Riley, Proc. Phys. Soc., **57**, 160 (1945)

[18] D. E. P. Vanpoucke, P. Bultinck, S. Cottenier and et al, J. Mater. Chem. A, **2**, 13723 (2014)

[19] N. Y. Mostafa, A. Badawi, S. I. Ahmed, Results Phys., **10**, 126 (2018)

[20] M. J. K. Kumar, J. T. Kalathi, J. Alloys Compd., **748**, 348 (2018)

[21] J. A. Kilner, B. C. H. Steele. Mass Transport in Anion-Deficient Fluorite Oxides. in: O. T. Sorensen. Ed. Nonstoichiometric Oxides. New York: Academic Press, 237 (1987)

[22] M. G. Shahraki, S. Ghorbanali, Microelectron. Reliab., **82**, 153 (2018)

[23] Z. F. Ma, Hebei University of Technology, Heibei (2005) in Chinese.

[24] R. E. Williford, W. J. Weber, R. D. Devanathan and et al, J. Electroceram., **3**, 409 (1999)

[25] E. K. Liu, B. S. Zhu, J. S. Luo. Semiconductor physics, Publishing House of Electronics Industry, Beijing, **7**, 126 (2017)

[26] Š. Csáki, J. Ondruška, V. Trnovcová and et al, Appl. Clay Sci., **157**, 19 (2018)